Journal of Applied Physics

Thermal conductivity model for nanofiber networks

Cite as: J. Appl. Phys. **123**, 085103 (2018); https://doi.org/10.1063/1.5008582
Submitted: 07 October 2017 . Accepted: 03 February 2018 . Published Online: 22 February 2018

Xinpeng Zhao, Congliang Huang, Qingkun Liu, Ivan I. Smalyukh, and Ronggui Yang

AIP Publishing

Thermal conductivity model for nanofiber networks

Xinpeng Zhao,[1] Congliang Huang,[1,2] Qingkun Liu,[3] Ivan I. Smalyukh,[3,4] and Ronggui Yang[1,4,5,a)]

[1]*Department of Mechanical Engineering, University of Colorado, Boulder, Colorado 80309, USA*
[2]*School of Electrical and Power Engineering, China University of Mining and Technology, Xuzhou 221116, China*
[3]*Department of Physics, University of Colorado, Boulder, Colorado 80309, USA*
[4]*Materials Science and Engineering Program, University of Colorado, Boulder, Colorado 80309, USA*
[5]*Buildings and Thermal Systems Center, National Renewable Energy Laboratory, Golden, Colorado 80401, USA*

(Received 7 October 2017; accepted 3 February 2018; published online 22 February 2018)

Understanding thermal transport in nanofiber networks is essential for their applications in thermal management, which are used extensively as mechanically sturdy thermal insulation or high thermal conductivity materials. In this study, using the statistical theory and Fourier's law of heat conduction while accounting for both the inter-fiber contact thermal resistance and the intrinsic thermal resistance of nanofibers, an analytical model is developed to predict the thermal conductivity of nanofiber networks as a function of their geometric and thermal properties. A scaling relation between the thermal conductivity and the geometric properties including volume fraction and nanofiber length of the network is revealed. This model agrees well with both numerical simulations and experimental measurements found in the literature. This model may prove useful in analyzing the experimental results and designing nanofiber networks for both high and low thermal conductivity applications. *Published by AIP Publishing*. https://doi.org/10.1063/1.5008582

I. INTRODUCTION

Nanofiber networks of carbon nanotubes (CNTs) or metallic nanowires (MNWs) have been extensively used to build thermally and/or electrically conducting and/or insulating materials. For example, applications are found in highly conductive thermal interface materials,[1] super insulating aerogels,[2] flexible electronics,[3] high performance transistors,[4] and electrodes of both batteries and fuel cells.[5] Nanofiber networks can possess significantly improved mechanical properties through the interconnected nanofibers.[6–8] Similarly, it is straightforward to expect that such kinds of networks could possess high electrical conductivity[6,9] and high thermal conductivity.[10] For example, the thermal conductivity of oil[11] and epoxy[12] can be enhanced by approximately 150% after adding 1 vol. % of high thermal conductivity single-wall CNTs when networks are formed. Similarly, Wang *et al.* showed a 10-times enhancement of thermal conductivity by adding only ∼0.9 vol. % copper nanowires into the polyacrylate matrix.[1] It is interesting to note that the enhancement of thermal conductivity using copper nanowires is much larger than that using CNTs, despite the much lower thermal conductivity of individual copper nanowires (200–300 W $m^{-1}K^{-1}$)[13] as compared to that of single-wall CNTs (∼3000 W $m^{-1}K^{-1}$).[14] This suggests that the contact resistance between nanofibers (CNTs or MNWs) might play an important role in the thermal transport through the networks. In contrary to the networks being used as highly thermal conductive materials, nanofiber networks have also been used to build thermal insulation materials. For example, the thermal conductivity of the random networks can be as low as ∼0.1 W $m^{-1}K^{-1}$ with 10–20 vol. % CNTs[15,16] or even lower for the CNT aerogel (∼0.06 W $m^{-1}K^{-1}$) with 0.3 vol. % CNTs.[2] These two extreme cases of using CNTs for both high and low thermal conductivity materials indicate that thermal transport in nanofiber networks depends on both their thermal properties, such as the thermal conductivity of a single nanofiber and the contact resistance of inter-fiber contact and the geometric properties, such as the volume fraction, the aspect ratio, and the orientation distribution of nanofibers. Developing a theoretical model that can be broadly applied to predict the thermal conductivity of nanofiber networks with a large set of physical variables, including both thermal and geometric properties, is not only fundamentally important to understand the heat transfer mechanisms within nanofiber networks, but also critical to enable many applications of nanofiber networks.

The intrinsic thermal resistance of nanofibers and the inter-fiber thermal contact resistance together determine the thermal conductivity of nanofiber networks. Earlier models focused mainly on the geometric factors such as heat transfer pathways, the volume fraction, and the aspect ratio of the nanofibers.[17–21] Such models paid very little attention to the effects of inter-fiber contact resistance. Recently, it was found that inter-fiber contact resistance has a noticeable effect on the thermal conductivity of fibrous materials[22–24] and CNT networks.[25] As a result, most of the modeling works on the thermal conductivity of CNT networks consider only heat transfer through contacts but neglect the thermal resistance along CNTs due to the very high thermal conductivity of a single CNT. On the other hand, Volkov and Zhigilei found that when the thermal conductivity of a single CNT is small, heat conduction through a CNT can strongly

a)E-mail: ronggui.yang@colorado.edu

influence the thermal conductivity of the random CNT networks.[25] It is well understood now that both the heat conduction through the nanofibers and inter-fiber contact thermal resistance need to be taken into account when modeling the thermal conductivity of nanofiber networks. In addition, the orientation distributions of the nanofibers in the network would affect the thermal conductivity of nanofiber networks.[26] In this paper, we develop a theoretical framework to analyze the thermal conductivity of nanofiber networks by considering both the inter-fiber contact thermal resistance and the intrinsic thermal resistance of nanofibers. The thermal conductivity is predicted as a function of the geometry parameters such as the volume fraction, nanofiber size, and the orientation distribution of the nanofibers. The scaling relationship describing dependence of thermal conductivity on the geometry parameters is also derived based on the newly developed model.

II. MODEL

A. Statistical description of a nanofiber network

Figure 1(a) shows a geometric illustration of a three-dimensional (3D) nanofiber network composed of straight nanofibers with uniform diameter D and length L. Here, we define the aspect ratio $r = L/D$ and assume $r \gg 1$. The cross-sectional area of a single nanofiber is $A_0 = \pi D^2/4$ and the volume fraction occupied by the nanofibers is assumed to be V_f. The total cross-sectional area of the network is defined as A_z. Figure 1(b) shows a typical structural element in the network in which χ is the angle formed between two arbitrary oriented nanofibers. The average contact number $\langle N_c \rangle$ is defined statistically to count the mean number of contacts of a nanofiber. The areal number density of the nanofiber through the cross-section A_z is assumed to be n_s. As shown in Fig. 1(c), the polar and azimuthal angles (θ, ϕ) are used to define the orientation of an arbitrary nanofiber. The orientation distribution function (ODF) $\Omega(\theta, \phi)$ describes the probability of finding the orientation of a nanofiber in the element of a unit sphere $\sin\theta d\theta d\phi$. The following normalization condition needs to be satisfied:

$$\int_{\theta_{min}}^{\theta_{max}} \int_{\phi_{min}}^{\phi_{max}} \Omega(\theta, \phi) \sin\theta d\phi d\theta = 1, \tag{1}$$

where θ_{min} and θ_{max} are the lower and upper limits of θ; ϕ_{min} and ϕ_{max} are the lower and upper limits of ϕ. For simplicity, we assume $\phi_{min} = 0$ and $\phi_{max} = \pi$ in this study.

The thermal conductivity of nanofiber networks is closely related to both the average contact number $\langle N_c \rangle$ which describes the connection of a network and the areal number density n_s which characterizes the concentration of nanofibers. Obviously, $\langle N_c \rangle$ and n_s are determined by the parameters such as the nanofiber size, volume fraction V_f, and ODF $\Omega(\theta, \phi)$. The $\langle N_c \rangle$ is the average of $N_c(\theta, \phi)$ over all possible values of (θ, ϕ), where $N_c(\theta, \phi)$ is defined as the number of contacts of a nanofiber with orientation distribution (θ, ϕ). According to the analysis by Pan,[27] $\langle N_c \rangle$ can be calculated as

$$\langle N_c \rangle = \frac{8 r V_f J(\theta, \phi)}{\pi + 4 V_f J(\theta, \phi) K(\theta, \phi)}, \tag{2}$$

where $\langle \cdot \rangle$ means the average value and $J(\theta, \phi)$ and $K(\theta, \phi)$ represent the mean value of $\sin\chi$ and $1/\sin\chi$, respectively (see the Appendix).[27]

As shown in Fig. 1(a), the areal number density n_s of the nanofibers penetrating the cross-section A_z with direction $\theta = 0$, is the summation over all possible values of $\nu(\theta = 0, 0 \le \phi \le \pi)$,

$$n_s = \int_0^{\pi} \nu(\theta = 0, \phi) d\phi, \tag{3}$$

where $\nu(\theta, \phi)$ is the areal number density of the cross-section in direction (θ, ϕ) (see the Appendix).[28] For the structure with $0 \le \theta_{min} < \frac{\pi}{2} < \theta_{max} \le \pi$, $n_s = V_f/2A_0$, and if the network is unidirectionally orientated in one direction (e.g., vertical alignment, $\theta_{min} = \theta_{max} = 0\, or\, \pi$), we have $n_s = V_f/A_0$.

B. Heat transfer analysis

In reality, nanofiber networks usually co-exist with gas or a matrix material, heat transfer through the gas or the

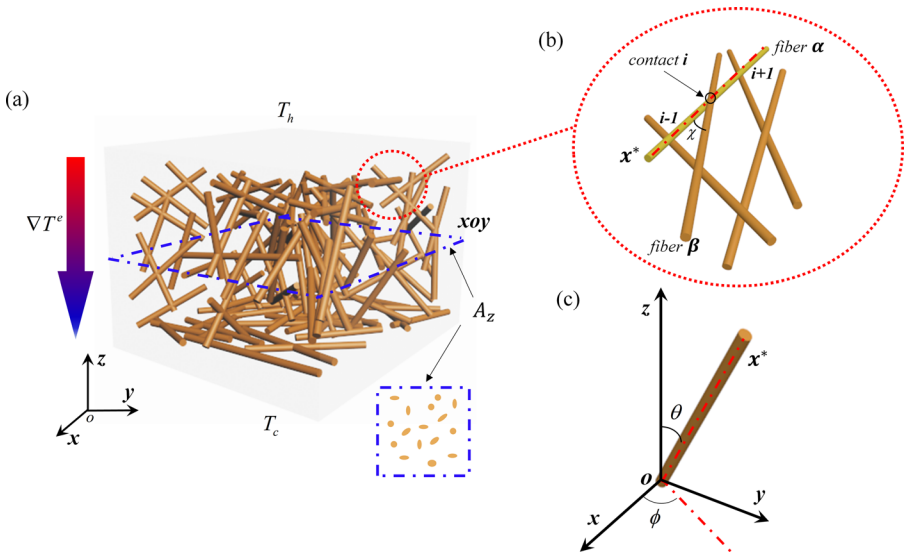

FIG. 1. Schematic of a nanofiber network. (a) A 3D nanofiber network under a temperature difference with high temperature T_h on the top and low temperature T_c at the bottom. (b) Contacts in the nanofiber network. The heat transfer through the contact between nanofiber α and nanofiber β is described by Eq. (8). (c) The orientation of a single nanofiber in the 3D space is described by polar and azimuthal angles (θ, ϕ).

matrix material and the infrared thermal radiation can make important contributions to the effective thermal conductivity of network based materials such as aerogels[2,29,30] or composites.[1,11] This work focused only on the heat conduction through the networks, which aims to guide the network design for thermal management. As shown in Fig. 1(a), a constant temperature gradient ∇T^e is assumed in the z direction. According to Fourier's law of heat conduction, the effective thermal conductivity of the network is given by

$$k_e = -\frac{Q_z}{A_z \nabla T^e}, \tag{4}$$

where Q_z is the total heat flow through A_z in the xoy plane. Q_z can also be written as the summation of the heat flow through every individual nanofiber across A_z in the z direction,

$$Q_z = \sum_{\alpha=1}^{n_s A_z} Q_\alpha = -n_s A_z |\langle Q_\alpha \rangle|, \tag{5}$$

where $|\langle Q_\alpha \rangle|$ is the ensemble averaged net heat flow through a single nanofiber, and the negative sign means that the direction of Q_z is negative z. By assuming that all contacts have the same thermal contact resistance and the heat flows in or out of the nanofiber through half of the contacts, we then have

$$|\langle Q_\alpha \rangle| = \left\langle \sum_{T_{\beta_j} > T_{\alpha_i}} h\left(T_{\beta_j} - T_{\alpha_i}\right) \right\rangle = k_0 A_0 \frac{\langle N_c \rangle}{2} Bi \frac{\langle \Delta T_{\alpha\beta} \rangle}{L}, \tag{6}$$

where h is the thermal conductance of the inter-fiber contact [Fig. 1(b)], which is the inverse of the thermal contact resistance, α_i means the ith contact along nanofiber α, β_j means the jth contact along nanofiber β, $\langle \Delta T_{\alpha\beta} \rangle = \left\langle \left| T_{\alpha_i} - T_{\beta_j} \right| \right\rangle$ is the average temperature difference in contacts between an arbitrary pair of nanofibers, $Bi = hL/k_0 A_0$ is Biot number, and k_0 is the thermal conductivity of the nanofiber.[23,24]

Substituting Eqs. (4) and (6) into Eq. (5), the following relationship between the effective thermal conductivity of the network k_e and the thermal conductivity of an individual nanofiber k_0 is obtained,

$$\frac{k_e}{k_0} = n_s A_0 \frac{\langle N_c \rangle}{2} Bi \frac{\langle \Delta T_{\alpha\beta} \rangle}{\nabla T^e} \frac{1}{L}. \tag{7}$$

Note that in Eq. (7) the value of $\langle \Delta T_{\alpha\beta} \rangle / \nabla T^e$ is an unknown and is determined by the competition between inter-fiber thermal contact resistance and thermal resistance from the nanofibers.

In a next step, the efforts are focused on finding $\langle \Delta T_{\alpha\beta} \rangle / \nabla T^e$ from the temperature distribution along the individual nanofiber and the network. Because the aspect ratio of the nanofiber is very high, it is reasonable to assume that the heat transfer along the nanofiber is one-dimensional (1D). For any of the nanofibers which do not touch the hot and cold surface, according to the energy balance at the ith contact along nanofibers α as shown in Fig. 1(b), the following equation can be written as:

$$k_0 A_0 \frac{T_{\alpha_i} - T_{\alpha_{i-1}}}{\Delta L_{\alpha_{i-1,i}}} + k_0 A_0 \frac{T_{\alpha_i} - T_{\alpha_{i+1}}}{\Delta L_{\alpha_{i,i+1}}} + h\left(T_{\alpha_i} - T_{\beta_j}\right) = 0, \tag{8}$$

where T_{α_i}, $T_{\alpha_{i-1}}$, and $T_{\alpha_{i+1}}$ are the temperature of the contact i, contact $(i-1)$, and contact $(i+1)$ on nanofiber α, and T_{β_j} is the temperature of contact j on nanofiber β [Fig. 1(b)], $\Delta L_{\alpha_{i-1,i}}$ is the distance between contact $(i-1)$ and contact i on nanofiber α, and $\Delta L_{\alpha_{i,i+1}}$ is the distance between contact i and contact $(i+1)$ on nanofiber α. In Eq. (8), the first and the second terms represent the heat flow along the nanofiber, while the third term is the heat transfer from nanofiber α to nanofiber β through the contact. Following a similar procedure, the energy balance equations are developed for other contacts on nanofiber α. As shown in Fig. 1(a), the direction of the heat flow is from the hot surface to the cold surface. The general temperature distribution along an individual nanofiber is that temperature decreases from the end closer to the top hot surface to the end closer to the bottom cold surface. To make the problem solvable, it is reasonable to assume that heat flows in the nanofiber from the end closer to the hot surface and flows out through the other end [this assumption is validated by our numerical simulations as shown in Fig. 3(b)]. We have thus assumed a constant average temperature gradient $\left\langle \left| \frac{dT}{dx^*} \right| \right\rangle = \frac{|\langle Q_\alpha \rangle|}{k_0 A_0}$ along the nanofiber.[25] Then

$$\frac{\left\langle \left| \frac{dT}{dx^*} \right| \right\rangle_M}{\langle \Delta T_{\alpha\beta} \rangle} = \frac{\langle N_c \rangle}{2} \frac{Bi}{L}, \tag{9}$$

where M means the middle point of a nanofiber.

Combining the assumed constant temperature gradient along each individual nanofiber with the assumption that a constant temperature gradient is applied in the z direction, the temperature distribution along nanofiber α can be expressed as a function of its z-coordinate,[25,31]

$$T(z_{\alpha_i}) = T_c + \nabla T^e z_{\alpha_M} + \frac{\left\langle \left| \frac{dT}{dx^*} \right| \right\rangle_M (z_{\alpha_i} - z_{\alpha_M})}{\langle |\cos\theta| \rangle}, \tag{10}$$

where T_c is the temperature of the network at $z = 0$, z_{α_M} and z_{α_i} are the z-coordinates of the middle point and ith contact on nanofiber α, and θ is the angle between the direction of a nanofiber and the direction of macroscopic heat transfer. The temperature $T(z_{\beta_j})$ of the jth contact on the nanofiber β can also be obtained, following a similar method. Thus, the average temperature difference at the contact between nanofibers α and β can be found using the difference of $T_\alpha(z_{\alpha_i})$ and $T_\beta(z_{\beta_j})$

$$\frac{\langle \Delta T_{\alpha\beta} \rangle}{\langle H \rangle} = \nabla T^e - \frac{\langle N_c \rangle}{2} \frac{Bi \langle \Delta T_{\alpha\beta} \rangle}{L} / \langle |\cos\theta| \rangle, \tag{11}$$

where $\langle H \rangle$ is the average center-to-center distance of the two connected nanofibers in the z direction (see the Appendix),

$$\langle H\rangle = \int_{-L/2}^{L/2}\int_{-L/2}^{L/2} dx_\alpha^* dx_\beta^* \int\int |z_\alpha - z_\beta|\Omega(\theta,\phi)\Omega(\theta,\phi)d\Omega_\alpha d\Omega_\beta$$
$$= \frac{\int_{-L/2}^{L/2}\int_{-L/2}^{L/2} dx_\alpha^* dx_\beta^* \int_{\theta_{min}}^{\theta_{max}} \sin\theta_\alpha d\theta_\alpha \int_{\theta_{min}}^{\theta_{max}} \sin\theta_\beta \left|x_\alpha^*\cos\theta_\alpha - x_\beta^*\cos\theta_\beta\right| d\theta_\beta}{\left(\cos\theta_{min} - \cos\theta_{max}\right)^2}. \quad (12)$$

Substituting Eq. (11) into Eq. (7), the effective thermal conductivity normalized by the thermal conductivity of fiber, k_e/k_0, is written as

$$\frac{k_e}{k_0} = n_s A_0 \frac{Bi\langle N_c\rangle}{2\langle|\cos\theta|\rangle L/\langle H\rangle + Bi\langle N_c\rangle}\langle|\cos\theta|\rangle. \quad (13)$$

Equation (13) is also valid for two-dimensional (2D) nanofiber networks. As shown in Fig. 1(c), the 3D network becomes 2D if $\phi = \pi/2$. It can be seen that Eq. (13) is closely related to the ODF of the networks. Table I lists the parameters for the 3D random ($0 \le \theta \le \pi$, $0 \le \phi \le \pi$) and 2D random ($0 \le \theta \le \pi$, $\phi = \frac{\pi}{2}$) networks (see the Appendix).

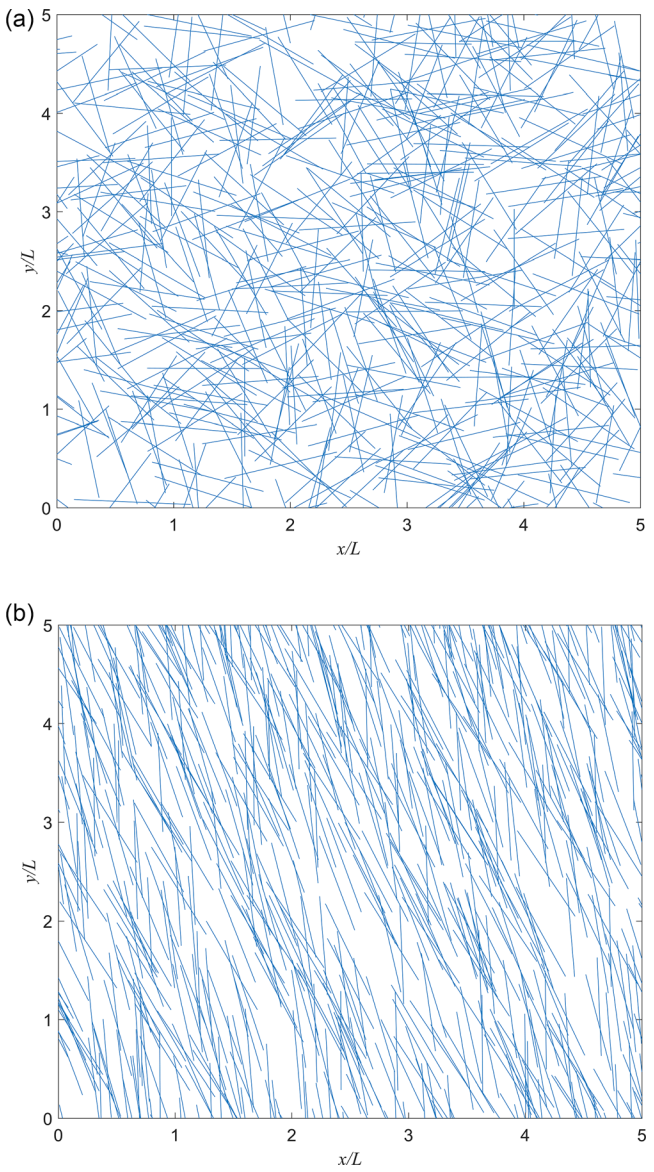

FIG. 2. Examples of the simulated random network ($0 < \theta < \pi$) and preferred orientation network ($0 < \theta < \pi/6$) in which $r = 500$ and $D = 3$ nm. The size of the computation domains is $L_h/L = 5$.

III. MODEL VALIDATION

A. Comparisons with numerical simulations

To validate the analytical model we derived in Sec. II, numerical simulations for thermal transport in nanofiber networks are conducted. To reduce the computational costs, the 2D networks with uniform size (length L and diameter D) of nanofibers are constructed. The arrangement of the nanofiber network is realized by generating two random numbers that determine the start position of each nanofiber inside the simulation domain, while a third random number is generated for the distribution angle θ according to the orientation distribution function. With the start position and the orientation θ, the end position of the nanofiber can be calculated easily based on the length of the nanofiber. If the end position of a nanofiber is outside the simulation domain, the point of intersection between the nanofiber and the domain boundary will be set as the end position of the nanofiber. This process is repeated until the volume fraction (area fraction in 2D) of the network is equal to the desired value. Figure 2 shows the examples of a simulated random network ($0 < \theta < \pi$) and a network with preferred orientation ($0 < \theta < \pi/6$), with the input parameters $V_f = 0.04$, $D = 3$ nm, and $r = 500$. The domain size ($L_h \times L_h$) of the simulated structures is nondimensionalized by the nanofiber length L.

In the simulation, each individual nanofiber in Fig. 2 is divided into 1D segments. A control volume heat balance analysis for each segment is performed by following a similar procedure used to derive Eq. (8). The top and bottom boundaries of the simulation domain are set as high temperature T_h and low temperature T_c. The dimensionless temperature $T^* = \frac{T-T_c}{T_h-T_c}$ in the simulations. The left and right boundaries of the simulation domain are assumed to be adiabatic. The two ends of nanofibers are assumed to be adiabatic if not touching another nanofiber. After the temperature distribution within the nanofiber network is obtained using the finite volume method (FVM), the effective thermal conductivity of the network is calculated as

$$k_e = \frac{\sum_{fibers} k_0 A_0 \left.\frac{dT}{dx^*}\right|_{z=0}}{A_d(T_h - T_c)/L_h}, \quad (14)$$

where A_d is the cross sectional area of the domain in the heat transfer direction. More details about the simulation model can

TABLE I. List of parameters for 3D and 2D random networks.

Geometry	Distribution angle, (θ, ϕ)	ODF, $\Omega(\theta, \phi)$	Average contact number,[27] $\langle N_c \rangle$	Areal number density, n_s	Center-to-center distance, $\langle H \rangle$	$\langle \lvert \cos\theta \rvert \rangle$
3D random	$0 \le \theta \le \pi, 0 \le \phi \le \pi$	$\frac{1}{2\pi}$	$\frac{4rV_f}{2+\pi V_f}$	$\frac{V_f}{2A_0}$	$0.1852L$	$\frac{2}{\pi}$
2D random	$0 \le \theta \le \pi, \phi = \frac{\pi}{2}$	$\frac{1}{\pi}$	$\frac{16\pi r V_f}{\pi^3 + 16\eta V_f}, \eta = ln[\cot(\arcsin(1/r)/2)]$	$\frac{4V_f}{\pi^2 A_0}$	$0.2307L$	$\frac{2}{\pi}$

be found in Ref. 32. For all the simulations in this paper, we keep the number of nanofibers in each simulation domain fixed to be around 500. The size of the calculation domains L_h/L ranges from 5 to 12 depending on the volume fraction and the aspect ratio of nanofibers. Numerical convergence tests are performed for all simulated cases. The calculated thermal conductivity for any of the nanofiber networks presented in this paper is the average result of 50 independent simulations.

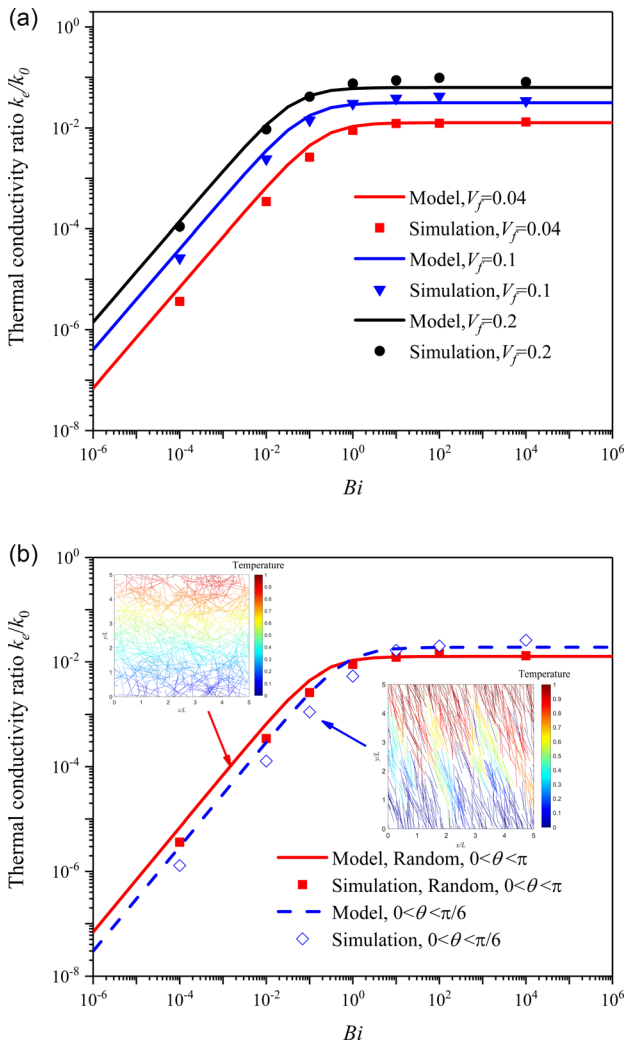

FIG. 3. (a) The effective thermal conductivity normalized to the thermal conductivity of the nanofiber, k_e/k_0 in the random nanofiber networks as a function of Bi according to Eq. (13) and numerical simulations, respectively. The input parameters are $r = 500$ and $D = 3$ nm. (b) Comparison of the thermal conductivity between random nanofiber networks $(0 < \theta < \pi)$ and nanofiber networks with preferred orientation $(0 < \theta < \pi/6)$ as a function of Bi. The two networks are assumed to have the same volume fraction $V_f = 0.04$, same aspect ratio $r = 500$, and same nanofiber diameter $D = 3$ nm. The insets in (b) show the example of simulated temperature distribution obtained for both the random nanofiber network and a nanofiber network with preferred orientation. The size of the simulation domain is $L_h/L = 5$ and the nanofibers are colored by non-dimensional temperature.

Figure 3 compares the effective thermal conductivities of the 2D networks obtained from the theoretical model [Eq. (13)] with those from numerical simulations, as a function of Bi number for different values of the volume fraction and different orientation distributions. To show the universality of the theoretical model we developed, the model is compared with the networks with Bi ranging from 10^{-4} to 10^4, where Bi represents the ratio of intrinsic thermal resistance of the nanofiber and inter-fiber contact resistance. Figure 3(a) shows that the effective thermal conductivity k_e of nanofiber networks is strongly dependent on the Bi number and the volume fraction of the nanofibers. For $Bi \to 0$, the k_e decreases following a power law with the change of the thermal resistance of inter-fiber contacts. However, when $Bi \to \infty$, the k_e becomes a constant which indicates that the effect of inter-fiber contact resistance vanishes and the k_e is only determined by the thermal resistance of the nanofiber. The volume fraction of the nanofibers influences k_e in the whole range of Bi values. Figure 3(b) compares the effective thermal conductivity k_e of random nanofiber networks $(0 < \theta < \pi)$ with those of nanofiber networks with preferred orientation $(0 < \theta < \frac{\pi}{6})$. When $Bi \to 0$, the effective thermal conductivity k_e of the random nanofiber networks is larger because of a larger average contact number $\langle N_c \rangle$. However, as $Bi \to \infty$, the effective thermal conductivity k_e of the networks with preferred orientation becomes larger due to the effect of orientation distribution.

B. Comparisons with experimental data

Figure 4 compares the predictions of the theoretical model with the experimental data from the literature for three kinds of nanofiber networks:[1,2,33–38] (1) CNT networks where CNTs have very high intrinsic thermal conductivity ($\sim 10^3$ W m^{-1}K^{-1}) but poor inter-fiber contact conductance (10–10^3 pW K^{-1}).[14,15] It is known that k_0 for an individual CNT can range from around 200 to 6000 W m^{-1}K^{-1},[14] depending on its length, diameter, chirality, tortuosity, and other factors. Here, $k_0 = 1000$ W m^{-1}K^{-1} is chosen for all the CNT networks (data points 1, 2, and 3 in Fig. 4). According to Prasher *et al.*[15] and Yamada *et al.*,[34] the inter-fiber thermal conductance h is ~50 pW K^{-1} for the CNT with diameter 1.4 nm, and h is ~15 000 pW K^{-1} when the diameter is 100 nm. Molecular simulations in the literature[39,40] show that inter-fiber thermal conductance has a positive correlation with the contact area (diameter) of nanofibers; thus h of point 1($D = 0.93$ nm) in Fig. 4 is chosen based on the diameter of the CNT (Table II). (2) Metallic

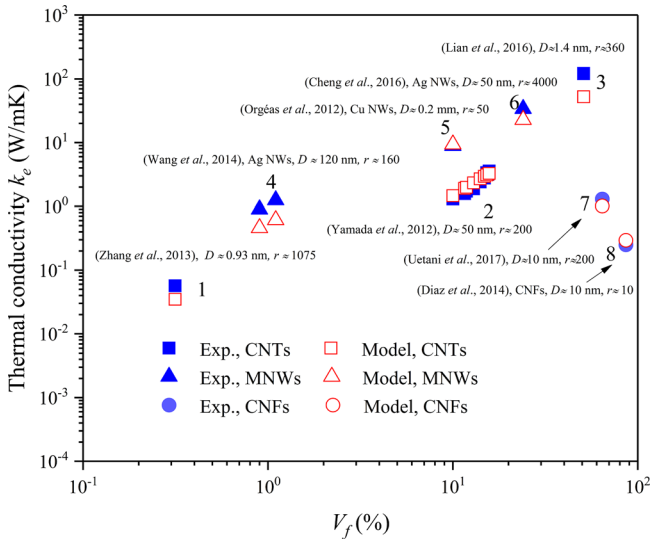

FIG. 4. Comparison between the theoretical model and the experimental data available in the literature. Three kinds of nanofiber networks are selected: (1) CNT networks, (2) MNW networks, and (3) CNF networks; Solid and open data points are for experimental data and the model, respectively.

nanowire networks where silver and copper nanowires (data points 4, 5, and 6 in Fig. 4) have high thermal conductivities ($\sim 10^2$ W m^{-1}K^{-1}) and excellent inter-fiber contact conductance ($\sim 10^5$ pW K^{-1}).[41] Here, k_0 ranges from 200 to 400 W m^{-1}K^{-1} on the basis of the diameter of MNWs.[13] (3) Cellulose nanofiber networks (CNFs) (data points 7 and 8 in Fig. 4) where nanofibers have low intrinsic thermal conductivity ($\sim 10^1$ W m^{-1}K^{-1}) and intermediate inter-fiber contact conductance ($\sim$973–1300 pW K^{-1}).[37] In CNF networks, neighboring CNFs are connected by much stronger hydrogen bonds than the van der Waals interactions in CNT networks. The molecular dynamics simulations from Diaz *et al.*[37] give the value of $k_0 = 5.7$ W m^{-1}K^{-1} and $h = 1000$ pW K^{-1}. Details about the experimental data and parameters in the theoretical model can be found in Table II. Figure 4 shows that results from the present model agree well with the experimental results for a broad range of Bi and the volume fraction. This demonstrates that our model can capture well the competition effects of both intrinsic thermal conductance of the nanofiber and inter-fiber contact resistance on the thermal conductivity of nanofiber networks.

IV. DEPENDENCE ON GEOMETRIC PARAMETERS

To characterize the effects of physical and geometric factors including the inter-fiber contact resistance, intrinsic thermal resistance of nanofibers, volume fraction, aspect ratio, and the orientation distribution on the effective thermal conductivity, a new parameter $Bi_T = \langle N_c \rangle Bi$ is defined according to Volkov and Zhigilei.[25] Eq. (13) is then reduced to

$$\frac{k_e}{k_0} = n_s A_0 \frac{Bi_T}{2\langle|\cos\theta|\rangle L/\langle H\rangle + Bi_T}\langle|\cos\theta|\rangle, \tag{15}$$

where Bi_T is the ratio of thermal resistance of the nanofiber L/k_0A_0 to the total inter-fiber contact resistance $1/h\langle N_c\rangle$ of all contacts in a nanofiber network. Unlike Bi which is a local characteristic number for an individual junction, Bi_T can be referred to as a global dimensionless quantity to characterize the ratio of the intrinsic thermal resistance of nanofibers and the contact resistance of the contacts in the network. Depending on the values of Bi_T, the heat transfer mechanisms in the nanofiber networks can be divided into different regimes.

(1) When a nanofiber network has a low volume fraction, a large aspect ratio or a large inter-fiber contact resistance, $Bi_T \ll 1$ is satisfied. Equation (15) is then reduced to

$$k_e = \frac{n_s\langle N_c\rangle\langle H\rangle}{2}h. \tag{16}$$

After substituting $\langle N_c\rangle$ [Eq. (2)] and $\langle H\rangle$ [Eq. (12)] into Eq. (16), we obtain

$$k_e \propto V_f^2 L^2. \tag{17}$$

Equation (17) indicates that the thermal conductivity of the nanofiber network is independent of the thermal conductivity of the single nanofiber and is only determined by the inter-fiber contact resistance and its geometry when $Bi_T \ll 1$. Equation (17) agrees well with the analytical model and mesoscopic simulation results from Volkov and Zhigilei[42] in which only the heat transfer through inter-fiber contacts is considered. The above trends are also validated by the numerical simulations in Fig. 5. For example, when $h = 5.0$ pW K^{-1} [Fig. 5(a), red line], the quadratic trend $k_e \propto L^b$, where $b = 2$, works well for both $V_f = 0.04$ and $V_f = 0.2$ for aspect ratio r varying from 100 to 1000. In Fig. 5(b), when $Bi = 10^{-4}$, $k_e \propto V_f^a$, where $a = 2$, is seen from the results

TABLE II. Details of the experimental data and selected parameters for the theoretical model.

Data	Material	Diameter, D(nm)	Length, L(μm)	Aspect ratio, r	Volume fraction, V_f(%)	Thermal conductivity, k_0(W m^{-1}K^{-1})	Inter-fiber conductance, h(pW K^{-1})	L_m (μm)
1	CNT[2]	0.93	1.0	1075	0.314	1000	25	/
2	CNT[34]	100	10	200	10-15.7	1000	1.5×10^4	10
3	CNT[35]	1.4	1.0	360	50.9	1000	50	/
4	MNW[1]	120	20	160	0.9–1.1	200	3×10^5	/
5	MNW[38]	0.2×10^6	10×10^3	50	10	400	1.1×10^{12}	/
6	MNW[33]	50	200	4000	24.0	300	0.52×10^5	/
7	CNF[36]	10	2	200	64.3	5.4	1000	2
8	CNF[37]	10	0.1	10	86.2	5.4	1000	2

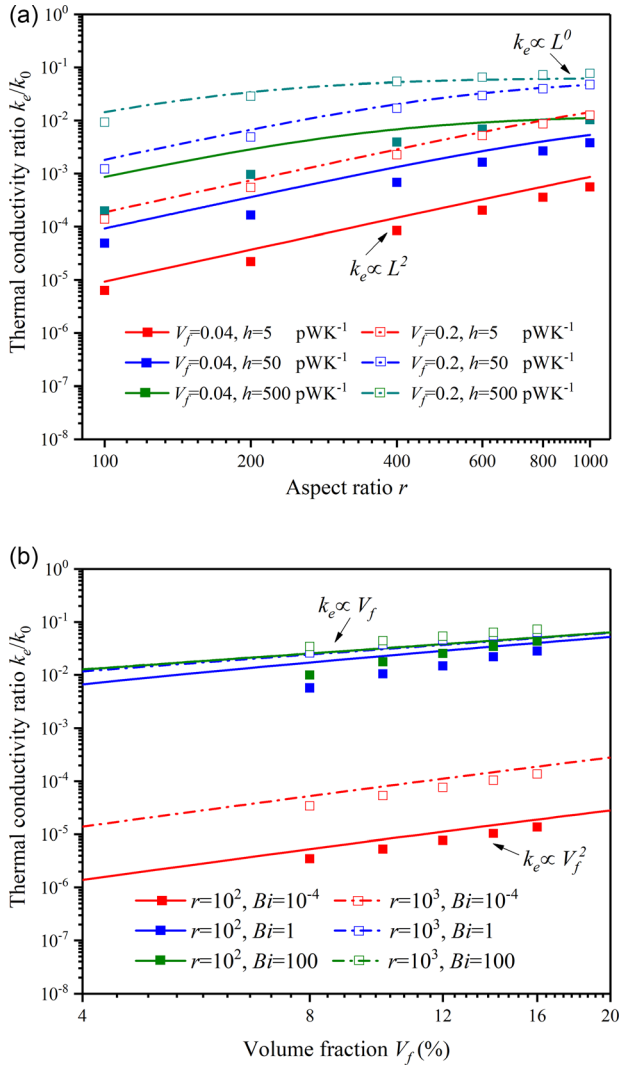

FIG. 5. The effective thermal conductivity of random nanofiber networks normalized to the thermal conductivity of nanofiber, k_e/k_0, from the theoretical model (lines) and numerical simulations (symbols) as a function of aspect ratio, r(100–1000) and V_f(0.04–0.2). The diameters of the nanofibers are all assumed to be 3 nm. The chosen parameters in the figure are to show the transition from $Bi_T \ll 1$ to $Bi_T \gg 1$. (a) $k_e \propto L^b$, where b decreases from 2 to 0 with the increase of r, h, and V_f; (b) $k_e \propto V_f^a$, where a decreases from 2 to 1 with the increase of r, Bi, and V_f.

of both $r = 100$ and $r = 1000$ (red solid and dashed lines). When the volume fraction or the aspect ratio of the nanofibers is small, computational simulations can generate some isolated nanofibers that do not contribute to the heat transfer of the network. Thus, it is noticed that the results from our analytical model are larger than the simulations, especially for the cases with high contact conductance [e.g., $V_f = 0.04$, $h = 500\,\mathrm{pW\,K^{-1}}$ in Fig. 5(a) and $r = 10^2$, $Bi = 100$ in Fig. 5(b)].

(2) When the nanofiber network has a high volume fraction or a small inter-fiber contact resistance, $Bi_T \gg 1$ is satisfied. Equation (15) can then be simplified as

$$k_e = n_s A_0 \langle|\cos\theta|\rangle k_0. \tag{18}$$

For the vertical aligned network ($\langle|\cos\theta|\rangle = 1.0$ and $n_s = V_f/A_0$), Eq. (18) reduces to the series thermal conductivity model, i.e., $k_e = V_f k_0$. When the nanofibers in the network are completely randomly distributed ($\langle|\cos\theta|\rangle = 2/\pi$ and $n_s = V_f/2A_0$), Eq. (18) can be simplified as $k_e = V_f k_0/\pi$, which agrees well with the theoretical estimation $k_e = V_f k_0/3$ for the 3D random network in Refs. 15 and 43. Because $n_s \propto V_f$, we now have

$$k_e \propto V_f. \tag{19}$$

Equation (19) indicates that the thermal conductivity of the nanofiber network is proportional to the volume fraction of the nanofibers and is independent of the nanofiber length. As shown in Fig. 5(a), the k_e becomes independent of the nanofiber length as r increases from 400 to 1000 when $h = 500$ pW K^{-1} (green line). In Fig. 5(b), by comparing the results for $r = 100$, $Bi = 100$ (green line) with those for $r = 1000$, $Bi = 100$ (pink lines), the linear dependence of k_e on V_f is clearly observed.

(3) For the intermediate case $Bi_T \sim 1$, the effective thermal conductivity can be written as

$$k_e \propto V_f^a L^b, \quad 1 < a < 2,\ 0 < b < 2. \tag{20}$$

For example, in Fig. 5(a), when both cases of $V_f = 0.04$, $h = 500\,\mathrm{pW\,K^{-1}}$ (green line) and $V_f = 0.2$, $h = 50\,\mathrm{pW\,K^{-1}}$ (blue line), the power exponent b decreases as r increases. This is because as the nanofiber length increases, Bi increases, which results in non-negligible thermal resistance of the nanofibers. In Fig. 5(b), as Bi increases from 10^{-4} to 100, the power exponent a changes from 2 to 1, for both cases where $r = 100$ and $r = 1000$.

The predictions of the theoretical model and the numerical simulations have shown the scaling relation $k_e \propto V_f^a L^b$. However, it is difficult to observe such a scaling relation from the experimental data in Fig. 4 directly. To verify the scaling relation with experimental data, in Fig. 6 we rearrange the experimental data as a function of V_{fe} which is an

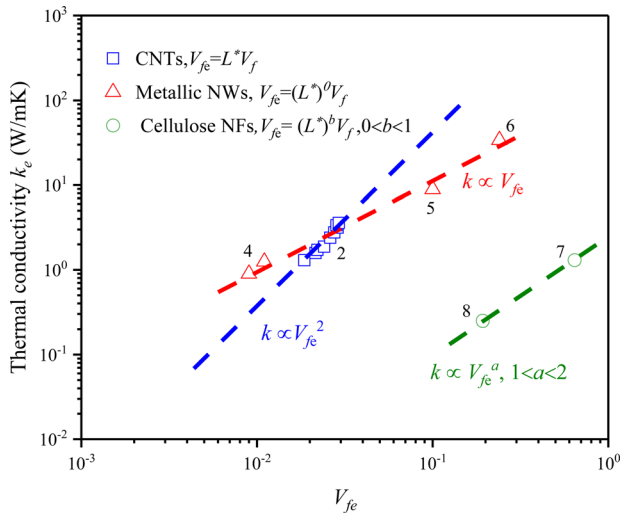

FIG. 6. Scaling law of thermal conductivity of nanofiber networks as a function of volume fraction and nanofiber length. The V_{fe} is an effective volume fraction defined as $V_{fe} = (L^*)^{b^*} V_f$, $0 \le b^* \le 1$, $L^* = L/L_m$. The relationship for CNT, MNW, and CNF networks can be written as: (a) CNT networks, $b^* = 1$, $k_e \propto V_{fe}^2$. (2) MNW networks, $b^* = 0$, $k_e \propto V_{fe}$. (3) CNF networks, $k_e \propto V_{fe}^{a^*}$, $0 < b^* < 1$, $1 < a^* < 2$. Note that $a^* = a$, $a^* b^* = b$.

effective volume fraction normalized by the length of the nanofiber, i.e., $V_{fe} = (L^*)^{b^*} V_f$, $0 \le b^* \le 1$, $L^* = L/L_m$, where L_m is the maximum length of the nanofibers in the networks (Table II). According to Eq. (16), when $Bi_T \ll 1$, the diameter and inter-fiber contact resistance also influence the thermal conductivity of the networks. Thus, only the CNT networks with the same size are chosen in Fig. 4. Because of the weak inter-fiber thermal coupling (large inter-fiber thermal contact resistance), k_e shows a quadratic dependence on V_{fe} in Fig. 6, which agrees well with the conclusion that $k_e \propto V_f^2$ when $Bi_T \ll 1$. The lower inter-fiber thermal contact resistance in random MNW network makes the k_e of MNW networks to be independent of the MNW length. Thus, in Fig. 6, k_e increases as V_{fe} $(b^* = 0)$ increases. For a CNF network, both the thermal resistance of nanofibers and inter-fiber contact resistances contribute to the effective thermal resistance k_e, which can be written as $k_e \propto V_{fe}^{a^*}$, where $1 < a^* < 2$, $0 < b^* < 1$.

V. CONCLUSIONS

In summary, we have developed a theoretical framework to analyze the thermal conductivity of nanofiber networks by considering the competition between heat conduction through the nanofibers and the inter-fiber contact resistance, using the statistical description of the nanofiber network and the Fourier's law of heat conduction. The physical and geometric factors such as inter-fiber contact thermal resistance, intrinsic thermal resistance of nanofibers, volume fraction, aspect ratio, and orientation distribution are taken into consideration. The theoretical model is validated by comparing with both numerical simulations and experimental data. The dependence of thermal conductivity on the volume fraction and nanofiber length is found: (1) when the network has a low volume fraction, large aspect ratio, or large inter-fiber contact resistance, i.e., $Bi_T \ll 1$, the thermal conductivity is determined by the inter-fiber contact thermal resistance and shows a quadratic dependence on both the volume fraction and nanofiber length ($k_e \propto V_f^2 L^2$); (2) when the network has a high volume fraction or small inter-fiber contact resistance, i.e., $Bi_T \gg 1$, the thermal conductivity of the network is determined by the intrinsic thermal resistance of the nanofibers and shows linear dependence on the volume fraction ($k_e \propto V_f$); (3) For the intermediate cases, i.e., $Bi_T \sim 1$, the thermal conductivity of the network is determined by both the inter-fiber contact resistance and intrinsic thermal resistance of the nanofibers ($k_e \propto V_f^a L^b$, where $1 < a < 2$, $0 < b < 2$).This model may prove useful in analyzing the experimental results and designing nanofiber networks for both high and low thermal conductivity applications.

ACKNOWLEDGMENTS

This research was supported by the U.S. Department of Energy, Advanced Research Projects Agency-Energy Award No. DE-AR0000743. X. P. Zhao acknowledges the fruitful discussions with Dr. P. Q. Jiang and X. Qian. X. P. Zhao also thanks Z. Cheng in Iowa State University for providing the experimental data for the silver networks.

APPENDIX A: THREE DIMENSIONAL (3D) NETWORKS

(1) Orientation distribution function $\Omega(\theta, \phi)$

In this work, we assume $\phi_{min} = 0$ and $\phi_{max} = \pi$, according to Eq. (1), we have

$$\int_{\theta_{min}}^{\theta_{max}} \int_0^{\pi} \Omega(\theta, \phi) \sin\theta d\phi d\theta = 1. \tag{A1}$$

The orientation distribution function for 3D networks is

$$\Omega(\theta, \phi) = \frac{1}{\pi(\cos\theta_{min} - \cos\theta_{max})}. \tag{A2}$$

(2) $J(\theta, \phi)$, $K(\theta, \phi)$and average contact number $\langle N_c \rangle$

$J(\theta, \phi)$ is the mean value of $\sin\chi(\theta, \phi, \theta', \phi')$, where χ is the angle between the nanofiber with distribution (θ', ϕ') and the nanofiber with distribution (θ, ϕ). The expression of $J(\theta, \phi)$ is[27]

$$J(\theta, \phi) = \int_{\theta_{min}}^{\theta_{max}} \int_0^{\pi} \Omega(\theta', \phi') \sin\chi(\theta, \phi, \theta', \phi') \sin\theta' d\phi' d\theta', \tag{A3}$$

where

$$\sin\chi(\theta, \phi, \theta', \phi') = \sqrt{1 - (\cos\theta\cos\theta' + \sin\theta\sin\theta'\cos(\phi - \phi'))^2}. \tag{A4}$$

Because of the independence of θ and ϕ,[27] we have

$$J(\theta, \phi) = J(0, 0) = \int_{\theta_{min}}^{\theta_{max}} \int_0^{\pi} \Omega(\theta', \phi') \sin\chi(0, 0, \theta', \phi') \sin\theta' d\phi' d\theta' \tag{A5}$$

and

$$\sin\chi(0, 0, \theta', \phi') = \sin\theta'. \tag{A6}$$

We can further write $J(\theta, \phi)$ as

$$J(\theta, \phi) = \int_{\theta_{min}}^{\theta_{max}} \int_0^{\pi} \frac{\sin\theta'^2}{\pi(\cos\theta_{min} - \cos\theta_{max})} d\phi' d\theta' = \frac{-\theta_{min} + \theta_{max} + \frac{1}{2}\sin 2\theta_{min} - \frac{1}{2}\sin 2\theta_{max}}{2(\cos\theta_{min} - \cos\theta_{max})}. \tag{A7}$$

$K(\theta, \phi)$ is the mean result of $\frac{1}{\sin\chi(\theta,\phi,\theta',\phi')}$, similar to $J(\theta, \phi)$,[27]

$$K(\theta, \phi) = \int_{\theta_{min}}^{\theta_{max}} \int_0^{\pi} \frac{\Omega(\theta', \phi')\sin\theta'}{\sin\chi(\theta, \phi, \theta', \phi')} d\phi' d\theta'. \tag{A8}$$

Because θ and ϕ are independent of all system parameters, we can have

$$K(\theta,\phi)=K(0,0)=\int_{\theta_{min}}^{\theta_{max}}\int_0^{\pi}\frac{\Omega(\theta',\phi')\sin\theta'}{\sin\chi(0,0,\theta',\phi')}d\phi'd\theta'$$
$$=\frac{\theta_{max}-\theta_{min}}{\cos\theta_{min}-\cos\theta_{max}}. \quad (A9)$$

For the 3D random network, $\theta_{max}=\pi$ and $\theta_{min}=0$, we have

$$J(\theta,\phi)=\frac{\pi}{4},\quad K(\theta,\phi)=\frac{\pi}{2}. \quad (A10)$$

Substituting the expressions of $J(\theta,\phi)$ and $K(\theta,\phi)$ into Eq. (2), we have the expression of average contact number of the 3D random network

$$\langle N_c\rangle=\frac{4rV_f}{2+\pi V_f}. \quad (A11)$$

(3) Areal number density n_s
The average number of fiber cut-ends on the plane whose normal direction is (Θ,Φ) can be calculated by the ratio of the total number of nanofibers traveling across the mean area of the fiber cut-ends. According to Ref. 28,

$$\nu(\Theta,\Phi)=\frac{V_f}{A_0}\Omega(\Theta,\Phi)\gamma(\Theta,\Phi), \quad (A12)$$

where V_f and A_0 are the volume fraction and cross-section of nanofibers, respectively. Here, $\gamma(\Theta,\Phi)$ is the statistical average value of $|\cos\chi|$ and can be calculated as

$$\gamma(\Theta,\Phi)=\int_{\theta_{min}}^{\theta_{max}}\int_0^{\pi}\Omega(\theta,\phi)\cos\chi(\theta,\phi,\Theta,\Phi)\sin\theta d\phi d\theta$$
$$=\int_{\theta_{min}}^{\theta_{max}}\frac{|\cos\theta|\sin\theta}{\cos\theta_{min}-\cos\theta_{max}}d\theta. \quad (A13)$$

Substituting Eqs. (A2) and (A13) into Eq. (A12), we have

$$\gamma(\Theta,\Phi)=\frac{1}{2}|\cos\theta_{min}+\cos\theta_{max}|, \quad (A14)$$

$$\nu(\Theta,\Phi)=\frac{V_f}{2\pi A_0}\frac{|\cos\theta_{min}+\cos\theta_{max}|}{\cos\theta_{min}-\cos\theta_{max}}, \quad (A15)$$

when $\theta_{min}\le\theta_{max}\le\frac{\pi}{2}$ or $\frac{\pi}{2}\le\theta_{min}\le\theta_{max}$, and

$$\gamma(\Theta,\Phi)=\frac{1}{2}(\cos\theta_{min}-\cos\theta_{max}), \quad (A16)$$

$$\nu(\Theta,\Phi)=\frac{V_f}{2\pi A_0}, \quad (A17)$$

when $\theta_{min}\le\frac{\pi}{2}\le\theta_{max}$.
The number density of the nanofiber penetrating the cross-section $A_z(\Theta=0,0\le\Phi\le\pi)$ is the summation of all possible values of $\nu(\Theta=0,0\le\Phi\le\pi)$, for the 3D random network, $\theta_{min}=0$ and $\theta_{max}=\pi$, then

$$n_s=\int_0^{\pi}\nu(0,\Phi)d\Phi=\frac{V_f}{2A_0}. \quad (A18)$$

(4) Average center to center distance $\langle H\rangle$
For the 3D random network

$$\langle H\rangle=\int_{-L/2}^{L/2}\int_{-L/2}^{L/2}dx_\alpha^*dx_\beta^*\int\int|z_\alpha-z_\beta|\Omega(\theta,\phi)\Omega(\theta,\phi)d\Omega_\alpha d\Omega_\beta$$
$$=\frac{1}{4}\int_{-L/2}^{L/2}\int_{-L/2}^{L/2}dx_\alpha^*dx_\beta^*$$
$$\times\int_0^{\pi}\int_0^{\pi}\left|x_\alpha^*\cos\theta_\alpha-x_\beta^*\cos\theta_\beta\right|d\cos\theta_\beta d\cos\theta_\alpha$$
$$=\frac{5}{27}L=0.1852L. \quad (A19)$$

APPENDIX B: TWO DIMENSIONAL (2D) NETWORKS

The results of 2D networks are a little different from those from 3D networks because of the zero thickness of the 2D system. When $\phi=\frac{\pi}{2}$, the 3D network changes to 2D network. The results for 2D networks can be obtained by substituting $\phi=\frac{\pi}{2}$ into the equations in Appendix A.

(1) Orientation distribution function $\Omega(\theta,\phi)$
On the basis of the normalization condition

$$\int_{\theta_{min}}^{\theta_{max}}\Omega\left(\theta,\frac{\pi}{2}\right)d\theta=1. \quad (B1)$$

Thus

$$\Omega\left(\theta,\frac{\pi}{2}\right)=\frac{1}{\theta_{max}-\theta_{min}}. \quad (B2)$$

(2) $J(\theta,\phi)$, $K(\theta,\phi)$and average contact number $\langle N_c\rangle$
Substituting Eqs. (B1) and (B2) into Eqs. (A3), (A4), and (A8), we have the expressions of $J(\theta,\phi)$ and $K(\theta,\phi)$ in 2D cases

$$J\left(\theta,\frac{\pi}{2}\right)=\frac{\cos\theta_{min}-\cos\theta_{max}}{\theta_{max}-\theta_{min}}, \quad (B3)$$

$$K\left(\theta,\frac{\pi}{2}\right)=\frac{ln\left(\tan\left(\frac{\theta_{max}}{2}\right)\right)-ln\left(\tan\left(\frac{\theta_{min}}{2}\right)\right)}{\theta_{max}-\theta_{min}}. \quad (B4)$$

For 2D random networks, there is a singular point in Eq. (B4) when $\theta_{min}=0$ and $\theta_{max}=\pi$, so the limits of Eq. (B4) are set as[27]

$$arc\sin\left(\frac{1}{r}\right)\le\theta\le\pi-arc\sin\left(\frac{1}{r}\right). \quad (B5)$$

From Eq. (B5), we can see that the $arc\sin\left(\frac{1}{r}\right)\approx0$, when the aspect ratio of the nanofiber is very large ($r\gg1$). Thus, we have

$$J\left(\theta,\frac{\pi}{2}\right)=\frac{2}{\pi},\quad K\left(\theta,\frac{\pi}{2}\right)=\frac{2}{\pi}ln\left(\cot\left(\frac{arc\sin\left(\frac{1}{r}\right)}{2}\right)\right). \quad (B6)$$

The average contact number is

$$\langle N_c\rangle = \frac{16\pi r V_f}{\pi^3 + 16\eta V_f}, \quad \eta = ln[\cot(\arcsin(1/r)/2)]. \tag{B7}$$

(3) Areal number density n_s
For 2D networks , Eq. (A13) becomes

$$\gamma\left(\Theta,\frac{\pi}{2}\right) = \frac{V_f}{A_0}\int_{\theta_{min}}^{\theta_{max}} \Omega\left(\theta,\frac{\pi}{2}\right)\cos\chi\left(\theta,\frac{\pi}{2},\Theta,\frac{\pi}{2}\right)d\theta = \frac{V_f}{A_0}\int_{\theta_{min}}^{\theta_{max}} \frac{|\cos\theta|}{\theta_{max}-\theta_{min}}d\theta. \tag{B8}$$

When $\theta_{min} \le \theta_{max} \le \frac{\pi}{2}$ or $\frac{\pi}{2} \le \theta_{min} \le \theta_{max}$,

$$\gamma\left(\Theta,\frac{\pi}{2}\right) = \frac{V_f}{A_0}\frac{|\sin\theta_{min} - \sin\theta_{max}|}{\theta_{max}-\theta_{min}}, \tag{B9}$$

$$\nu\left(\Theta,\frac{\pi}{2}\right) = \frac{V_f}{A_0}\frac{|\sin\theta_{min} - \sin\theta_{max}|}{(\theta_{max}-\theta_{min})^2}. \tag{B10}$$

When $\theta_{min} \le \frac{\pi}{2} \le \theta_{max}$,

$$\gamma\left(\Theta,\frac{\pi}{2}\right) = \frac{1-\sin\theta_{min}}{\frac{\pi}{2}-\theta_{min}} + \frac{1-\sin\theta_{max}}{\theta_{max}-\frac{\pi}{2}}, \tag{B11}$$

$$\nu\left(\Theta,\frac{\pi}{2}\right) = \frac{V_f}{A_0(\theta_{max}-\theta_{min})}\left(\frac{1-\sin\theta_{min}}{\frac{\pi}{2}-\theta_{min}} + \frac{1-\sin\theta_{max}}{\theta_{max}-\frac{\pi}{2}}\right). \tag{B12}$$

For the 2D random network ($\theta_{min} = 0$ and $\theta_{max} = \pi$), the area number density cross cross-section $A_z(\Theta = 0, \Phi = \frac{\pi}{2})$ is

$$n_s = \nu\left(0,\frac{\pi}{2}\right) = \frac{4V_f}{\pi^2 A_0}. \tag{B13}$$

(4) Average center to center distance $\langle H\rangle$
For the 2D random network

$$\begin{aligned}\langle H\rangle &= \int_{-L/2}^{L/2}\int_{-L/2}^{L/2} dx_\alpha^* dx_\beta^* \times \int\int |z_\alpha - z_\beta|\Omega(\theta,\phi)\Omega(\theta,\phi)d\Omega_\alpha d\Omega_\beta \\ &= \frac{1}{\pi^2}\int_{-L/2}^{L/2}\int_{-L/2}^{L/2} dx_\alpha^* dx_\beta^* \times \int_0^\pi\int_0^\pi \left|x_\alpha^*\cos\theta_\alpha - x_\beta^*\cos\theta_\beta\right| d\theta_\beta d\theta_\alpha \\ &= 0.2307L.\end{aligned} \tag{B14}$$

[1] S. Wang, Y. Cheng, R. Wang, J. Sun, and L. Gao, ACS Appl. Mater. Interfaces **6**, 6481 (2014).
[2] K. J. Zhang, A. Yadav, K. H. Kim, Y. Oh, M. F. Islam, C. Uher, and K. P. Pipe, Adv. Mater. **25**, 2926 (2013).
[3] S. Park, M. Vosguerichian, and Z. Bao, Nanoscale **5**, 1727 (2013).
[4] G. J. Brady, A. J. Way, N. S. Safron, H. T. Evensen, P. Gopalan, and M. S. Arnold, Sci. Adv. **2**, e1601240 (2016).
[5] M. Tian, W. Wang, Y. Liu, K. L. Jungjohann, C. T. Harris, Y.-C. Lee, and R. Yang, Nano Energy **11**, 500 (2015).
[6] A. Allaoui, S. Bai, H. M. Cheng, and J. Bai, Composites Sci. Technol. **62**, 1993 (2002).
[7] A. Esawi, K. Morsi, A. Sayed, M. Taher, and S. Lanka, Composites Sci. Technol. **70**, 2237 (2010).
[8] F. H. Gojny, M. H. Wichmann, B. Fiedler, and K. Schulte, Composites Sci. Technol. **65**, 2300 (2005).
[9] W. Bauhofer and J. Z. Kovacs, Composites Sci. Technol. **69**, 1486 (2009).
[10] M. Biercuk, M. C. Llaguno, M. Radosavljevic, J. Hyun, A. T. Johnson, and J. E. Fischer, Appl. Phys. Lett. **80**, 2767 (2002).
[11] S. Choi, Z. Zhang, W. Yu, F. Lockwood, and E. Grulke, Appl. Phys. Lett. **79**, 2252 (2001).
[12] M. Bryning, D. Milkie, M. Islam, J. Kikkawa, and A. Yodh, Appl. Phys. Lett. **87**, 161909 (2005).
[13] C. Huang, Y. Feng, X. Zhang, J. Li, and G. Wang, Physica E **58**, 111 (2014).
[14] A. M. Marconnet, M. A. Panzer, and K. E. Goodson, Rev. Mod. Phys. **85**, 1295 (2013).
[15] R. S. Prasher, X. Hu, Y. Chalopin, N. Mingo, K. Lofgreen, S. Volz, F. Cleri, and P. Keblinski, Phys. Rev. Lett. **102**, 105901 (2009).
[16] Y. J. Heo, C. H. Yun, W. N. Kim, and H. S. Lee, Curr. Appl. Phys. **11**, 1144 (2011).
[17] S. T. Baxter, Proc. Phys. Soc. **58**, 105 (1946).
[18] N. E. Hager, Jr. and R. C. Steere, J. Appl. Phys. **38**, 4663 (1967).
[19] X. Cheng, A. M. Sastry, and B. E. Layton, J. Eng. Mater. Technol. **123**, 12 (2000).
[20] S. Y. Fu and Y. W. Mai, J. Appl. Polym. Sci. **88**, 1497 (2003).
[21] S. Kumar, J. Murthy, and M. Alam, Phys. Rev. Lett. **95**, 066802 (2005).
[22] J. P. Vassal, L. Orgéas, D. Favier, J. L. Auriault, and S. Le Corre, Phys. Rev. E **77**, 011303 (2008).
[23] J. P. Vassal, L. Orgéas, D. Favier, J. L. Auriault, and S. Le Corre, Phys. Rev. E **77**, 011302 (2008).
[24] J. Vassal, L. Orgéas, and D. Favier, Modell. Simul. Mater. Sci. Eng. **16**, 035007 (2008).
[25] A. N. Volkov and L. V. Zhigilei, Appl. Phys. Lett. **101**, 043113 (2012).
[26] L. Zhang, G. Zhang, C. Liu, and S. Fan, Nano Lett. **12**, 4848 (2012).
[27] N. Pan, Text. Res. J. **63**(6), 336 (1993).
[28] N. Pan and P. Gibson, *Thermal and Moisture Transport in Fibrous Materials* (Woodhead Publishing, 2006).
[29] H. Liu, Z. Y. Li, X. P. Zhao, and W. Q. Tao, Int. J. Heat Mass Transfer **95**, 1026 (2016).
[30] Z. Y. Li, H. Liu, X. P. Zhao, and W. Q. Tao, J. Non-Cryst. Solids **430**, 43 (2015).
[31] Y. Chalopin, S. Volz, and N. Mingo, J. Appl. Phys. **105**, 084301 (2009).
[32] S. Kumar, M. A. Alam, and J. Y. Murthy, J. Heat Transfer **129**, 500 (2007).
[33] Z. Cheng, M. Han, P. Yuan, S. Xu, B. A. Cola, and X. Wang, RSC Adv. **6**, 90674 (2016).
[34] Y. Yamada, T. Nishiyama, T. Yasuhara, and K. Takahashi, J. Therm. Sci. Technol. **7**, 190 (2012).
[35] F. Lian, J. P. Llinas, Z. Li, D. Estrada, and E. Pop, Appl. Phys. Lett. **108**, 103101 (2016).
[36] K. Uetani, T. Okada, and H. T. Oyama, ACS Macro Lett. **6**, 345 (2017).
[37] J. A. Diaz, Z. Ye, X. Wu, A. L. Moore, R. J. Moon, A. Martini, D. J. Boday, and J. P. Youngblood, Biomacromolecules **15**, 4096 (2014).
[38] L. Orgéas, P. J. Dumont, J.-P. Vassal, O. Guiraud, V. Michaud, and D. Favier, J. Mater. Sci. **47**, 2932 (2012).
[39] W. J. Evans, M. Shen, and P. Keblinski, Appl. Phys. Lett. **100**, 261908 (2012).
[40] H. Zhong and J. R. Lukes, Phys. Rev. B **74**, 125403 (2006).
[41] R. Venkatesh, J. Amrit, Y. Chalopin, and S. Volz, Phys. Rev. B **83**, 115425 (2011).
[42] A. N. Volkov and L. V. Zhigilei, Phys. Rev. Lett. **104**, 215902 (2010).
[43] C. W. Nan, R. Birringer, D. R. Clarke, and H. Gleiter, J. Appl. Phys. **81**, 6692 (1997).